Supporting Information

Polyoxometalate-Based Inorganic-Organic Hybrid $[Cu(phen)_2]_2[(\alpha\text{-}Mo_8O_{26})]$: A New Additive to Spiro-OMeTAD for Efficient and Stable Perovskite Solar Cells

Yayu Dong,† Yulin Yang,*,† Lele Qiu,† Guohua Dong,‡ Debin Xia,† Xianda Liu,† Mengru Li,† and Ruiqing Fan*,†

†MIIT Key Laboratory of Critical Materials Technology for New Energy Conversion and Storage School of Chemistry and Chemical Engineering, Harbin Institute of Technology, Harbin 150001, P.R. China

E-mail: ylyang@hit.edu.cn; fanruiqing@hit.edu.cn

‡College of Chemistry and Chemical Engineering, Qiqihar University, Qiqihar 161006, P.R. China

S1 Experimental Section

Measurements and Characterizations: The photocurrent-voltage (*J-V*) plots and impedance spectroscopy (EIS) were conducted at the open air with a CHI660D electrochemical work station and a solar simulator under AM 1.5 G sunlight produced by a 450 W xenon lamp, whose light intensity was adjusted with a standard Si reference cell (Oriel, 1 sun light intensity 100 mW/cm^2). Active area of solar cells is 0.06 cm^2. The scan rate of *J-V* plots and frequency of EIS are 20 mV/s and 1-10^5 HZ, respectively. The incident photo to electron efficiency (IPCE) spectra were carried out using the system installed a 300 W xenon lamp to give out the excitation beam. The given light was collected through a 1/4 monochromator (model 74125 Oriel Cornerstone 260, Newport, USA). Fourier transform infrared (FT−IR) spectra were collected on a PerkinElmer Spectrum 100 FT−IR spectrometer with samples prepared as KBr discs. X-ray diffraction (XRD) characteristics were performed using Shimadzu XRD-6000 X-ray Diffraction instrument with Cu−Kα radiation. Scan electron microscope (SEM) measurements were conducted by Rili SU 8000HSD Series Hitachi New Generation Cold Field Emission SEM. The AFM analysis were performed by using a Bruker Dimension ICONPT with Co/Cr tips. The given signal was ultimately collected by a lock-in amplifier. UV-vis absorption spectra were recorded by a Shimadu and SPECORD S600 spectrophotometer. Photoluminescence performance were investigated by steady-state fluorescence spectrometer FLS920. The PL emission intensity spectra were recorded by an FLS 920 luminescence spectrometer. The ESR spectra was measured using an X-band (9.69 GHz) Bruker ER083CS spectrometer at 300 K. Cyclic voltammetry (CV) was obtained using the Gamry electrochemical workstation with Pt plate as working electron, Pt slice as counter electrode, and Ag/AgCl electrode as reference electrode in tetrabutylammonium hexafluorophosphate (Bu_4NPF_6, 0.1 M) chlorobenzene solutions at a scan rate of 50 mV/s. The follow energy level calculation method were used to determine the HOMO according to the literature.[1,2]

$$E_{LUMO} = -(E^{Red} + 4.50 + 0.20) \quad (1)$$

$$E_{HOMO} = -(E^{Ox} + 4.50 + 0.20) \quad (2)$$

$$E_{HOMO} = E_g + E_{LUMO} \quad (3)$$

Mobility Measurements

Hole mobility was investigated by the space-charge-limited current (SCLC) method, which can be described by the following equation:

$$J = (9/8)\ \mu\ \varepsilon_o\ \varepsilon_r\ (V^2/d^3)$$

where J is the current density, μ is the hole mobility, ε_o is the vacuum permittivity (8.85×10^{-12} F/m), ε_r is the dielectric constant of the material (normally taken to approach 3 for organic semiconductors), V is the applied bias, and d is the film thickness.

S2 Single-crystal structure analysis

The collection of single-crystal X-ray analyses data were performed on a Bruker Apex II CCD equipped with a normal focus at 296K, sealed tube X-ray source (Mo-Kα radiation, λ = 0.71073 Å) operating at 50 kV and 30 mA. The structures were solved by direct methods and refined by full-matrix least-squares using the SHELXL-2014/7 program package. Anisotropic thermal parameters were used to refine all non-hydrogen atoms. A summary of the crystallographic data and structure determination for CMP is provided in Table S2. Selected bond lengths and angles for **CMP** are given in Table S3 and S4. Distances (Å) and angles (°) of hydrogen bonds for CMP are given in Table S5.

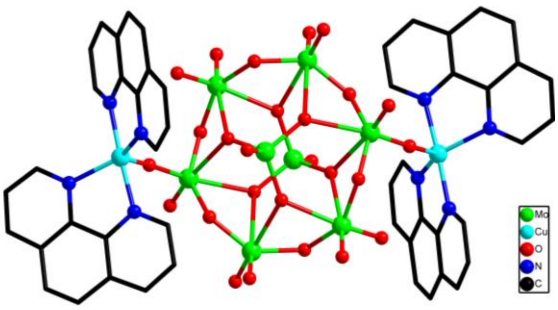

Fig. S1 The structure of CMP

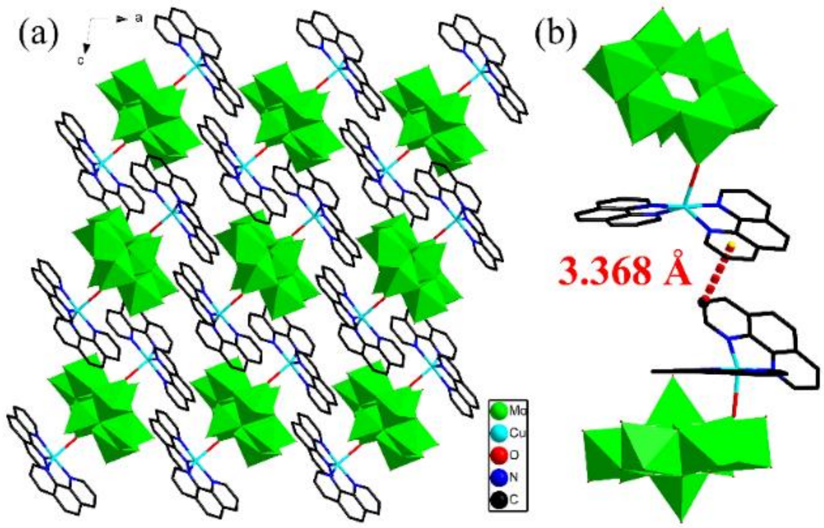

Fig. S2 (a) The 3D framework of CMP along the b-axis; (b) π-π stacking interactions between adjacent clusters

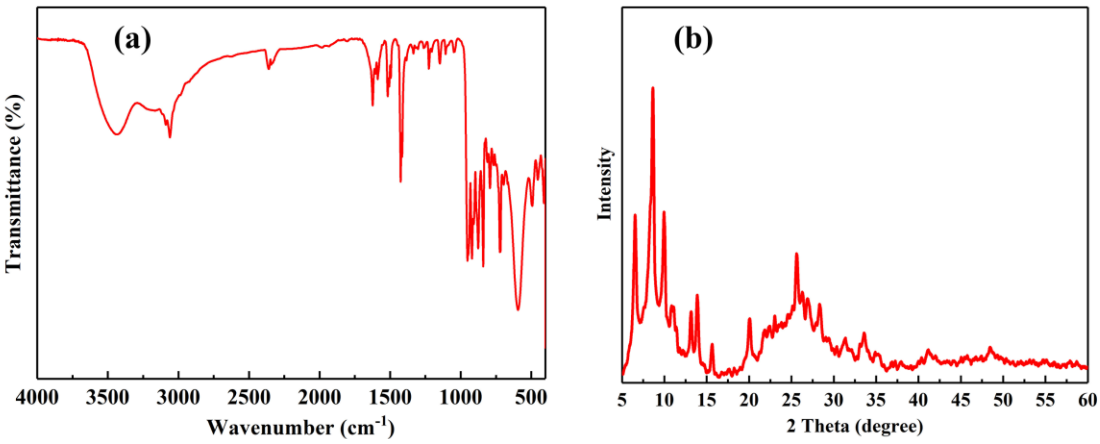

Fig. S3 (a) The FTIR spectrum of CMP; (b) The XRD pattern of CMP

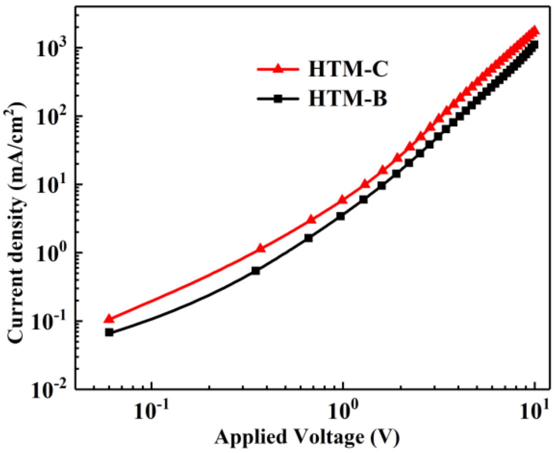

Fig. S4 The dark J-V curves of HTM-B and HTM-C based hole-only devices.

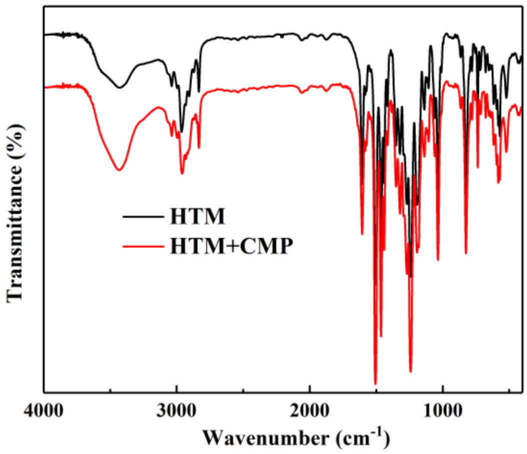

Fig. S5 The FTIR spectra of HTL doped with or without CMP

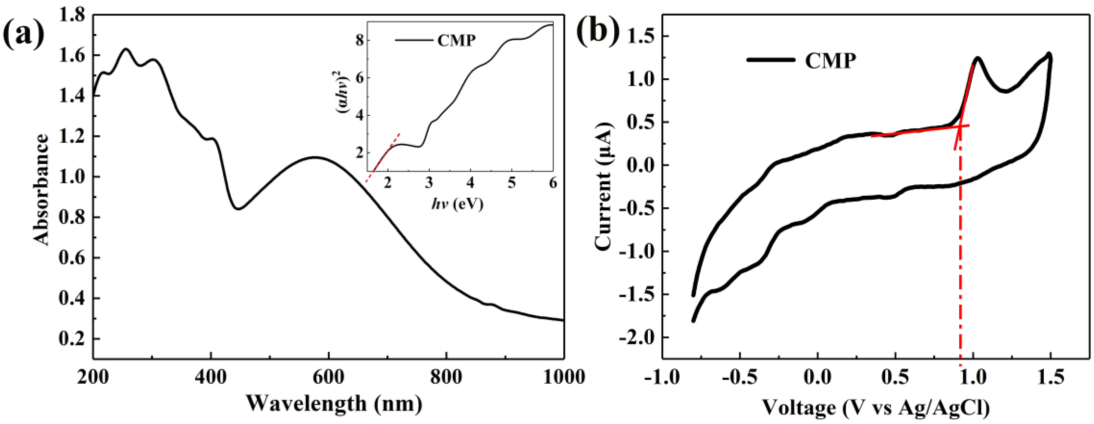

Fig. S6 The UV-vis spectrum and cyclic voltametry spectrum of the synthesized heteropolyacid CMP (a) UV-vis spectrum (the Inset is the tauc plot); (b) cyclic voltametry spectrum

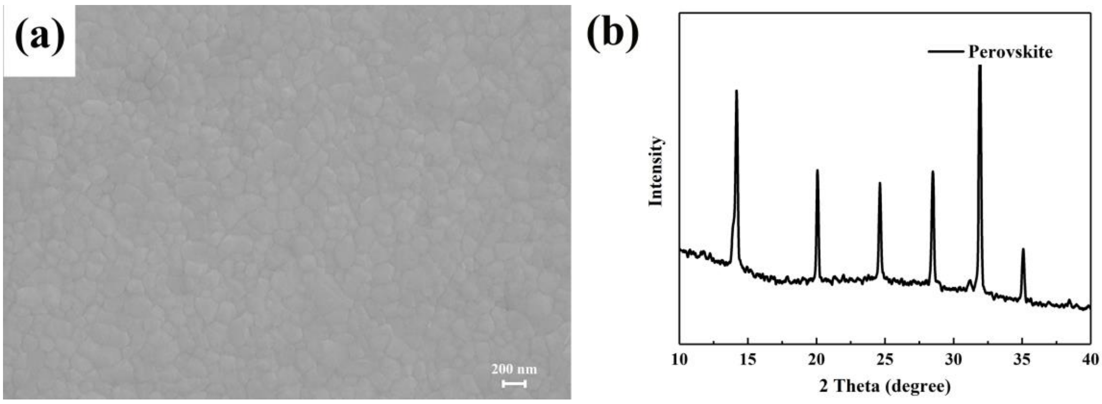

Fig. S7 (a) The SEM image and (b) XRD pattern of perovskite film

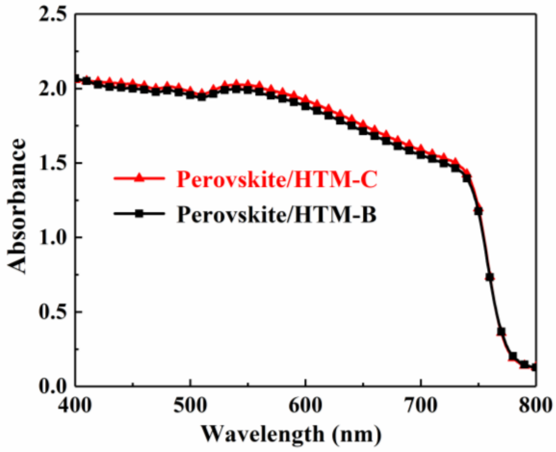

Fig. S8 The UV-vis absorption spectra of HTM-B and HTM-C

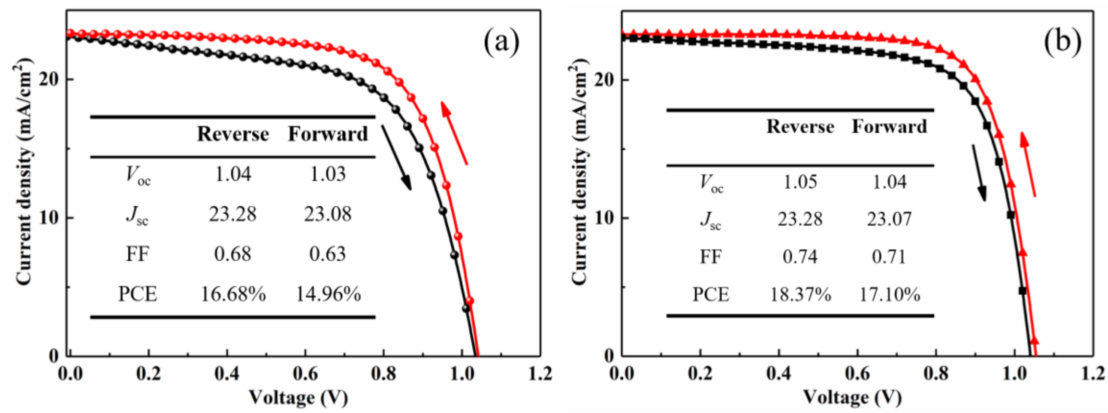

Fig. S9 The J-V curves of devices (a) HTM-B (b) HTM-C in the forward and reverse scanning directions

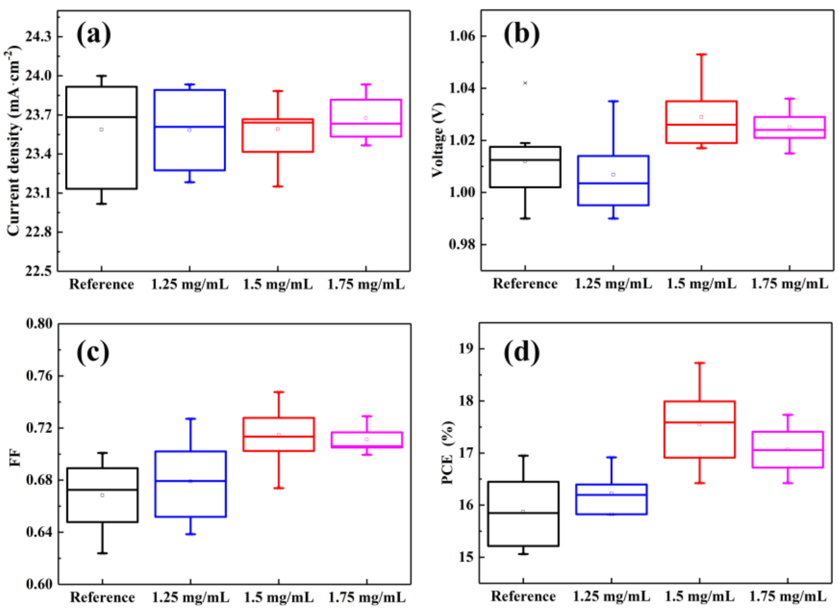

Fig. S10 Statistical distribution of the (a) Jsc (b) Voc (c) FF (d) PCEs for PSCs with different concentrations of CMP

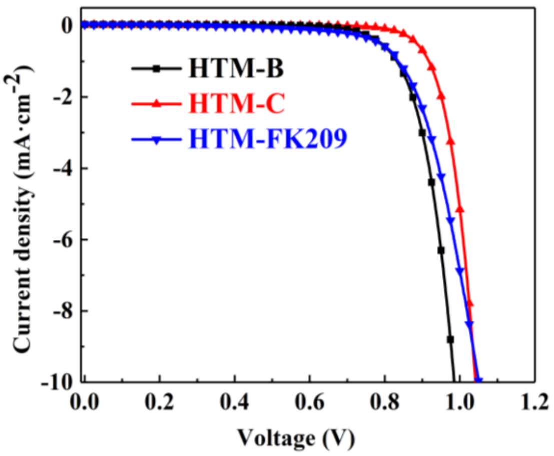

Fig. S11 The current density-voltage (J-V) curves of the optimal PSCs with different HTMs under dark

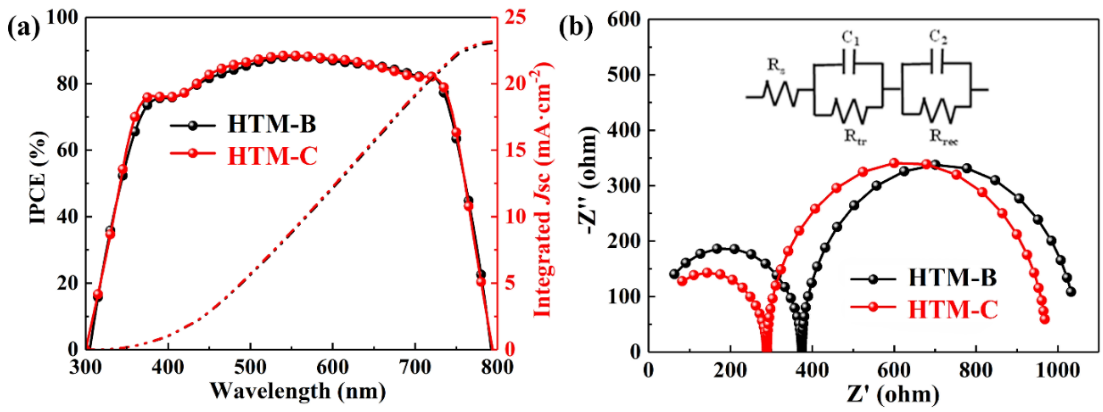

Fig. S12 (a) incident photo-to-current conversion efficiency spectra; (b) The EIS measurement spectra of the PSCs fabricated with or without CMP. The Inset of Figure d is the equivalent electrical circuits for fitting the EIS data

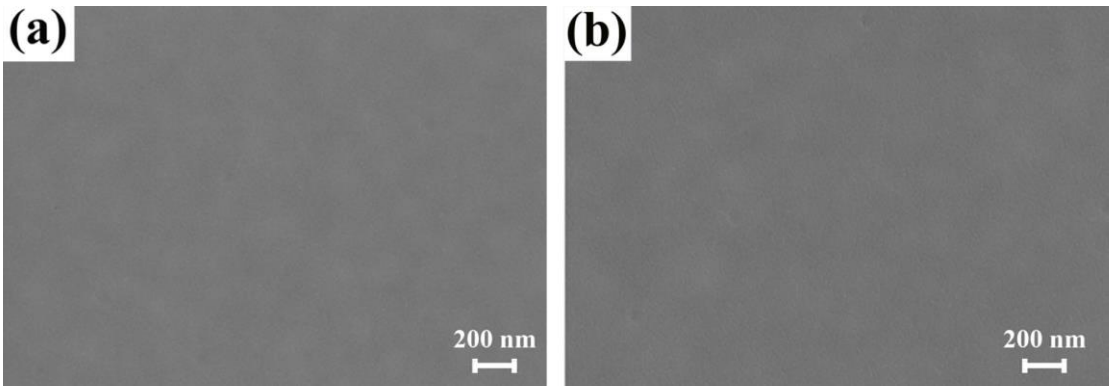

Fig. S13 The SEM image of HTL film (a) and with CMP (b)

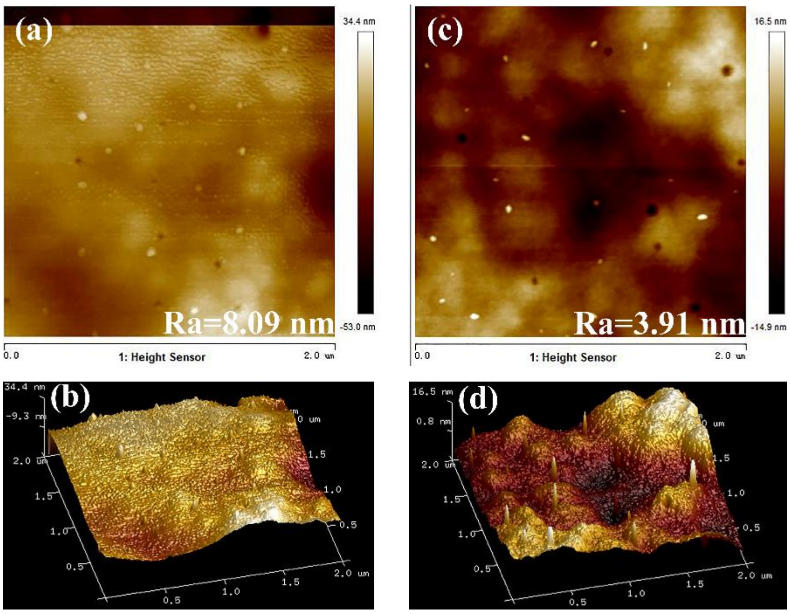

Fig. S14 Top view AFM images of (a) HTL; (b) 3D AFM images of HTL; (c) HTL with CMP; (d) 3D AFM images of HTL with CMP

Table S1 Carrier lifetime of corresponding devices with or without different complexes

Devices	τ_1	τ_2	A_1%	A_2%	τ(average)
Perovskite	0.81	6.07	87.19	12.81	5.49
Perovskite/HTL	0.71	6.87	73.53	26.47	3.57
Perovskite/HTL-CMP	0.79	5.40	86.80	13.20	3.14

Table S2 The Crystallographic data of CMP

Compound	**CMP**
Empirical formula	C48 H32 Cu2 Mo8 N8 O26
Formula weight	2031.44
Temperature (K)	296(2)
Crystal system	Monoclinic
Space group	P21/c
a (Å)	10.5018(6)
b (Å)	12.0953(7)
c (Å)	21.9996(13)
β (°)	97.989(1)
Volume ($Å^3$)	2767.3(3)
Z	2
Calculated density (Mg / m^3)	2.438

Absorption coefficient (mm^{-1})	2.597
F(000)	1956
Crystal size (mm^3)	0.11 x 0.12 x 0.13
Limiting indices	-12<=h<=12 -13<=k<=14 -26<=l<=21
Reflections collected	13937
Independent reflection	[R(int) = 0.028]
Max. and min. transmission	0.752 and 0.721
Refinement method	Full-matrix least-squares on F^2
Data / restraints / parameters	4925 / 1 / 415
Goodness-of-fit on F^2	1.03
Final R indices [I > 2sigma(I)][ab]	R1 = 0.0250, wR2 = 0.601
R indices (all data)	R1 = 0.0328, wR2 = 0.627

[a]$R1 = \Sigma||F_o| - |F_c||/\Sigma|F_o|$; $wR2 = \Sigma[w(F_o^2 - F_c^2)^2]/\Sigma[w(F_o^2)^2]^{1/2}$

Table S3 Selected bond lengths for CMP (Å)

Mo1-O4	1.928(2)	Mo2-O5_a	2.410(2)
Mo1-O6	2.367(3)	Mo3-O5	1.785(3)
Mo1-O14	1.687(3)	Mo3-O6	1.790(3)
Mo1-O15	1.698(2)	Mo3-O9	1.705(2)
Mo1-O1_a	1.925(2)	Mo3-O12	1.772(3)
Mo1-O5_a	2.343(2)	Mo4-O1	1.894(2)
Mo2-O2	1.895(2)	Mo4-O2	1.907(2)
Mo2-O4	1.888(2)	Mo4-O3	1.683(3)
Mo2-O10	1.689(3)	Mo4-O7	1.725(3)
Mo2-O11	1.695(3)	Mo4-O12	2.440(3)
Mo4-O6_a	2.389(3)	Cu1-N2	2.094(4)
Cu1-O7	2.192(2)	Cu1-N3	1.961(3)
Cu1-N1	1.972(3)	Cu1-N4	2.051(3)

Table S4 Selected bond angles (°) for CMP

O4-Mo1-O6	81.69(9)	O6-MO2 -O5	108.29(13)
O4-Mo1-O14	97.60(14)	O6-Mo3-O12	109.69(13)
O4-Mo1-O15	101.52(11)	O9-Mo3-O12	110.69(12)
O1_a-Mo1-O4	147.14(10)	O1-Mo4-O2	144.05(10)
O4-Mo1-O5_a	72.78(9)	O1-Mo4-O3	100.54(13)
O6-Mo1-O14	90.33(13)	O1-Mo4-O7	102.31(11)
O6-Mo1-O15	165.02(12)	O1-Mo4-O12	78.83(11)
O1_a-Mo1-O6	71.98(9)	O1-Mo4-O6_a	71.94(10)
O5_a-Mo1-O6	73.60(10)	O2-Mo4-O3	102.09(13)
O14-Mo1-O15	103.61(14)	O2-Mo4-O7	98.88(10)
O1_a-Mo1-O14	101.78(14)	O2-Mo4-O12	73.09(10)
O5_a-Mo1-O14	162.11(14)	O2-Mo4-O6_a	79.89(10)

O1_a-Mo1-O15	99.40(11)	O3-Mo4-O7	103.96(13)
O5_a-Mo1-O15	93.23(12)	O3-Mo4-O12	91.36(11)
O1_a-Mo1-O5_a	81.03(10)	O3-Mo4-O6_a	166.53(13)
O2-Mo2-O4	139.59(10)	O7-Mo4-O12	164.04(10)
O2-Mo2-O10	102.00(12)	O6_a-Mo4-O7	88.77(11)
O2-Mo2-O11	102.22(12)	O6_a-Mo4-O12	76.37(9)
O2-Mo2-O5_a	79.39(9)	O7-Cu1-N1	87.11(11)
O4-Mo2-O10	100.04(12)	O7-Cu1-N2	94.32(11)
O4-Mo2-O11	104.73(11)	O7-Cu1-N3	90.69(11)
O4-Mo2-O5_a	71.81(10)	O7-Cu1-N4	129.53(11)
O10-Mo2-O11	103.99(14)	N1-Cu1-N2	82.08(11)
O5_a-Mo2-O10	166.59(13)	N1-Cu1-N3	176.84(12)
O5_a-Mo2-O11	88.60(12)	N1-Cu1-N4	97.64(12)
O5-Mo3-O6	110.45(12)	N2-Cu1-N3	100.36(11)
O5-Mo3-O9	108.42(13)	N2-Cu1-N4	136.15(12)
O5-Mo3-O12	109.28(12)	N3-Cu1-N4	82.02(12)

Table S5 Distances and angles [Å, °] of hydrogen bonds for CMP

D–H···A	**d(D–H)**	**d(H···A)**	**d(D···A)**	**∠D–H···A**
C2-H2A···O9	0.93	2.56	3.161(5)	123
C2-H2A···O11	0.93	2.59	3.075(5)	113
C3-H3A···O9	0.93	2.59	3.181(5)	122
C7-H7A···O10	0.93	2.56	3.282(5)	135
C14-H14A···O9	0.93	2.51	3.072(5)	119
C19-H19A···O1	0.93	2.5	3.415(5)	166
C22-H22A···O15	0.93	2.6	3.519(5)	170
C24-H24A···O11	0.93	2.42	3.080(5)	127

(1) Lv, S.; Wang, Z. Y.; Gu, X.; Zhang, C.; Jian, Y. G.; Lin, H. Coordination polymer based perovskite device: matched energy levels and photocurrent enhancement in the absence or presence of methanol. *CrystEngComm*. **2017**, *19*, 7021–7030.

(2) Lee, D. Y.; Shinde, D. V.; Yoon, S. J.; Cho, K. N.; Lee, W.; Shrestha, N. K.; Han, S. H. Cu-Based Metal–Organic Frameworks for Photovoltaic Application. *J. Phys. Chem. C*, **2014**, *118*, 16328.